THE JOURNAL OF PHYSICAL CHEMISTRY LETTERS
A JOURNAL OF THE AMERICAN CHEMICAL SOCIETY

pubs.acs.org/JPCL Letter

The Impact of Spacer Size on Charge Transfer Excitons in Dion–Jacobson and Ruddlesden–Popper Layered Hybrid Perovskites

George C. Fish, Aaron T. Terpstra, Algirdas Dučinskas, Masaud Almalki, Loï C. Carbone, Lukas Pfeifer, Michael Grätzel, Jacques-E. Moser,* and Jovana V. Milić*

Cite This: *J. Phys. Chem. Lett.* 2023, 14, 6248–6254 Read Online

ACCESS | Metrics & More | Article Recommendations | Supporting Information

ABSTRACT: Organic materials can tune the optical properties in layered (2D) hybrid perovskites, although their impact on photophysics is often overlooked. Here, we use transient absorption spectroscopy to probe the Dion–Jacobson (DJ) and Ruddlesden–Popper (RP) 2D perovskite phases. We show the formation of charge transfer excitons in DJ phases, resulting in a photoinduced Stark effect which is shown to be dependent on the spacer size. By using electroabsorption spectroscopy, we quantify the strength of the photoinduced electric field, while temperature-dependent measurements demonstrate new features in the transient spectra of RP phases at low temperatures resulting from the quantum-confined Stark effect. This study reveals the impact of spacer size and perovskite phase configuration on charge transfer excitons in 2D perovskites of interest to their advanced material design.

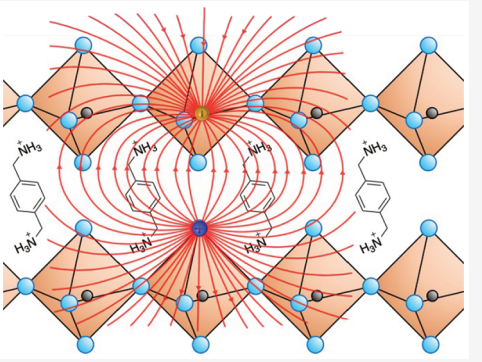

Lead halide perovskites have become one of the most attractive materials for optoelectronic applications over the past decade.[1−3] They have been used extensively in solar cells, with efficiencies of single junction devices reaching over 25%,[4] as well as in LEDs[5] and for lasing applications.[6] Characterized by the general formula ABX_3, they form an octahedral crystalline structure, where A is typically a methylammonium (MA^+), formamidinium (FA^+), or cesium (Cs^+) cation, among others; B represents a divalent metal ion, such as Pb^{2+} or Sn^{2+}; and X is a halide anion (Br^-, Cl^- or I^-).[3] By altering their composition, it is possible to change the resulting structure and optoelectronic properties.[7−9]

One issue associated with metal halide perovskites is their environmental stability and, in particular, their sensitivity to humidity.[10,11] To overcome this, hybrid two-dimensional (2D) perovskites have been successfully implemented.[2,12,13] In these systems, the A cation is replaced with a larger organic cation, one example being 2-phenylethylammonium (PEA), which inhibits the formation of the typical 3D structure. Instead, a layered (2D) structure forms that consists of layers of $\{PbI_6\}$ corner-sharing octahedra separated by the organic cations (i.e., spacers, *S*). 2D perovskites can be categorized by the crystallographic planes of the 3D parent structure, with <100> being the most common orientation. This group of 2D perovskites can be further subdivided into three categories, namely, Ruddlesden–Popper (RP), Dion–Jacobson (DJ), and alternating cation in the interlayer (ACI) phases.[14] The latter of these categories has, as of yet, only been formed when replacing alternate methylammonium cations with guanidinium.[15,16] The RP and DJ perovskites can be differentiated based on the valency of the spacer used, as RP forms typically with a monovalent spacer cation and DJ with a divalent spacer.[17,18] RP perovskites form a staggered structure, with the general formula $(S')_2A_{n-1}B_nX_{3n+1}$, whereby S' is a monovalent spacer and *n* is the number of perovskite layers. In contrast, the layers in DJ perovskites stack with no lateral displacement and commonly have the general formula $(S)A_{n-1}B_nX_{3n+1}$, where S is a divalent spacer cation.[2,19]

Despite demonstrating greater environmental stability compared to their 3D counterparts, phase purity is often an issue when fabricating 2D perovskites with an increasing thickness of perovskite layers ($n > 1$).[20] Due to the addition of the organic spacers and the possibility of changing the stacking structure, it is possible to tune the physical properties of 2D perovskites, such as the optical band gap and the exciton binding energy.[21−23] Significant work has been undertaken to develop and investigate various potential spacer molecules,[14] yet the impact of the spacer on photophysics is often overlooked.[19,23,24] To date, photophysical studies on 2D perovskites have utilized various techniques and covered

Received: April 25, 2023
Accepted: May 22, 2023

https://doi.org/10.1021/acs.jpclett.3c01125
J. Phys. Chem. Lett. 2023, 14, 6248–6254

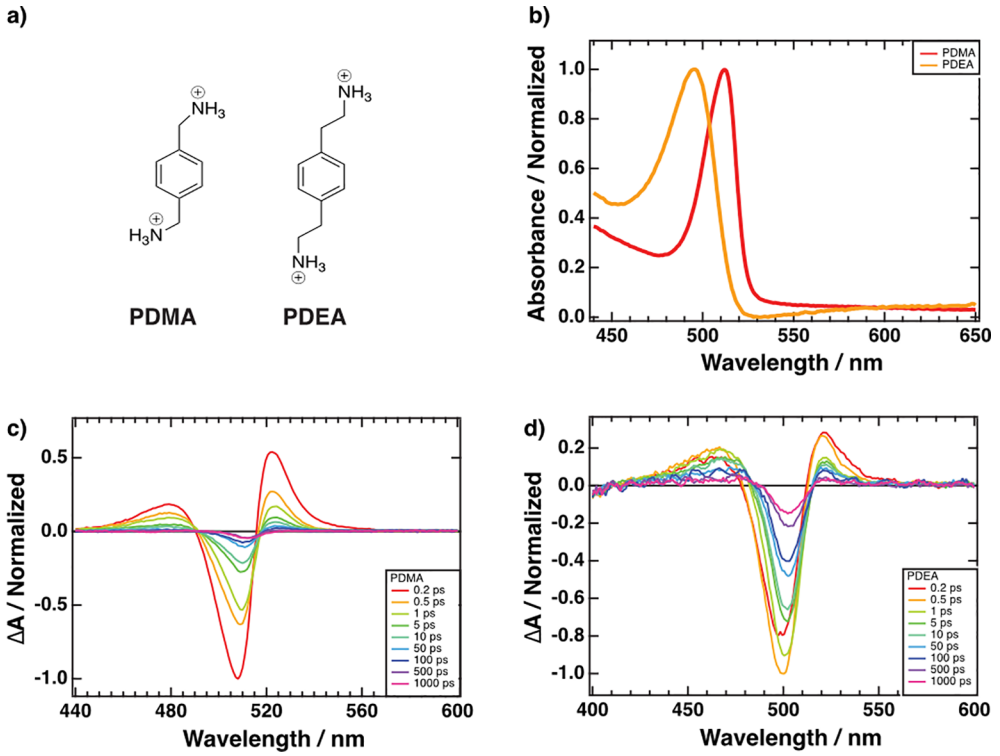

Figure 1. (a) Chemical structures of 1,4-phenylenedimethylammonium (PDMA) and 1,4-phenylenediethylammonium (PDEA) spacer cations. (b) Steady-state UV−vis absorption spectra of 2D perovskite thin films incorporating PDMA (red) and PDEA (orange) organic spacers within $SPbI_4$ 2D perovskite compositions (S = PDMA, PDEA). (c,d) Transient absorption spectra of PDMA (c) and PDEA (d) based 2D perovskites. Samples were excited at 390 nm with a fluence of 10 uJ/cm^2. The two spectra are normalized to the negative feature for the ease of comparison.

several areas, including the comparison of carrier dynamics between the representative Dion−Jacobson and Ruddlesden−Popper phases,[23] quantum confined Stark effect in 2D perovskites with different layers,[25] time-resolved THz spectroscopy to explore charge carrier evolution[26] and hot carrier cooling.[27] There is still uncertainty around the role of the spacer size and layer orientation on charge transfer species formed upon photoexcitation.

Here, we use transient absorption and electroabsorption spectroscopy to determine the impact of the spacer size and layer orientation on charge transfer excitons in 2D perovskites. Furthermore, temperature-dependent steady state and transient absorption techniques are used to further elucidate the impact of the interlayer distance on charge transfer exciton formation.

Two representative aromatic spacers were used to determine the impact of interlayer distance on the photophysics in 2D perovskites, namely, 1,4-phenylenedimethylammonium (PDMA) and 1,4-phenylenediethylammonium (PDEA). These spacers form Dion−Jacobson (DJ) perovskites, with the formula $(PDMA)PbI_4$ and $(PDEA)PbI_4$, which will be referred to by the abbreviation associated with their spacer moiety (Figure 1a).[28−30] We have also analyzed the 2-phenylethylammonium (PEA) based Ruddlesden−Popper (RP) perovskite phase for comparison, with the focus on the n = 1 2D perovskite compositions due to their phase purity.[28−30] The films were prepared using stoichiometric amounts of the precursors in a mixture of *N*,*N*-dimethylformamide and dimethyl sulfoxide (4:1 v/v) spin-coated on glass substrates followed by annealing, in accordance with the procedure detailed in the Supporting Information (SI).

To determine the phase purity of the PDMA and PDEA samples, the steady-state absorption spectra were measured (Figure 1b). The samples display singular sharp peaks at 495 (PDEA) and 510 nm (PDMA), which can be assigned to the excitonic band. Furthermore, an absence of peaks/features between 550 and 600 nm indicates that these 2D perovskite samples possess an n = 1 structure, with no higher-order (n > 1) phases present. This is important to establish as it means that we can expect the features in the transient absorption (TA) measurements to only arise from the n = 1 layer, and we can discount any contributions from higher-order phases.

With evidence of the phase purity of the samples studied, we carried out TA measurements at different fluences to assess whether the spacer size influenced the type of photogenerated species within the films. Excitation at 390 nm yielded the TA spectra for the two compositions (Figure 1c,d) that are similar in shape, with a negative bleaching feature flanked on either side by positive absorption features. The TA spectrum of PDMA-based 2D perovskites (Figure 1c) displays a negative feature at 508 nm that could be assigned to the ground state bleaching due to its similarity to the steady-state absorption spectrum. However, the peak exhibits a 5 nm red shift from 0.2 to 1000 ps over time. Therefore, it is evident that this negative feature has more than one contribution, with each contribution at a different time scale. We postulate that a second contribution to the negative feature at 508 nm could arise due to a photoinduced Stark effect, which could also be an explanation for the two positive features on either side. The kinetics of the three features (taken at 479, 508, and 522 nm; Figure S1, SI) show identical initial decays, implying that they each possess a contribution from the same process, thus

https://doi.org/10.1021/acs.jpclett.3c01125
J. Phys. Chem. Lett. 2023, 14, 6248−6254

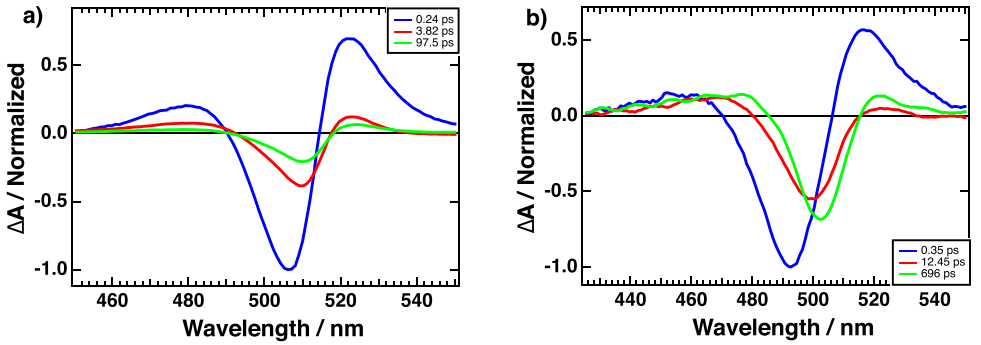

Figure 2. Decay-associated spectra (DAS) following global analysis of the TA spectra of (a) PDMA and (b) PDEA-based 2D perovskite thin films.

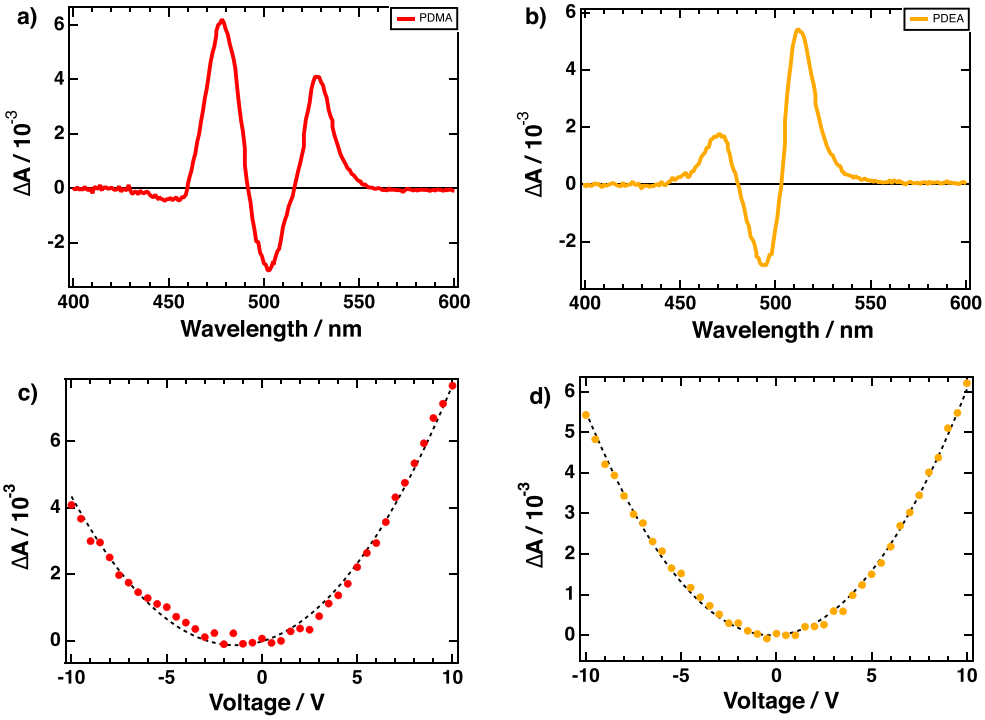

Figure 3. Electroabsorption spectra of 2D perovskites incorporating (a) PDMA and (b) PDEA spacers. Spectra were taken at an applied voltage of −10 V. Graphs showing the voltage dependence for the (c) PDMA and (d) PDEA samples were taken at 526 and 512 nm, respectively.

providing more evidence that it could be related to a photoinduced Stark effect.

The Stark effect occurs when an electric field causes a shift in the absorption spectrum of the sample. The impact of the electric field upon the frequency of the transition is given by the following equation (eq 1).[31]

$$\Delta\nu = -\Delta\mu\cdot E - \frac{1}{2}\Delta\alpha\cdot E^2 \tag{1}$$

Here, $\Delta\mu$ corresponds to the change in the dipole moment, $\Delta\alpha$, the change in the polarizability, and E is the photoinduced electric field. The change in the absorbance of a sample can then be expressed mathematically as a function of the frequency of the electronic transitions. A Taylor expansion of this yields the following expression (eq 2).

$$A(\nu, E) = A(\nu, E = 0) + \frac{dA}{d\nu}d\nu + \frac{1}{2}\frac{d^2A}{d\nu^2} + \ldots \tag{2}$$

By substituting the expression for the frequency (given by eq 1) in the expression, the following equation is obtained for the electroabsorption signal (eq 3).

$$EA = -\frac{dA}{d\nu}\Delta\mu\cdot E + \frac{1}{2}\frac{d^2A}{d\nu^2}E^2\cdot\Delta\mu^2 - \frac{1}{2}\frac{dA}{d\nu}E^2\cdot\Delta\alpha \tag{3}$$

As the first term is linear with respect to the electric field, it is 0 in isotropic systems. Therefore, this equation suggests that changes in the dipole moment, $\Delta\mu$, are associated with the second derivative of the absorption spectrum. On the other hand, changes in the polarizability, $\Delta\alpha$, are related to the first derivative of the absorption spectrum. In the case of a photoinduced Stark effect, the electric field is generated intrinsically upon photoexcitation.

By comparison of the shape of the PDMA TA spectrum to the first and second derivatives of its absorption spectrum (Figure S2, SI), it is evident that it closely resembles the second derivative. As a result, the photoinduced Stark effect arises from changes in the dipole moment. In contrast, the photoinduced field could arise from the formation of charge

https://doi.org/10.1021/acs.jpclett.3c01125
J. Phys. Chem. Lett. 2023, 14, 6248−6254

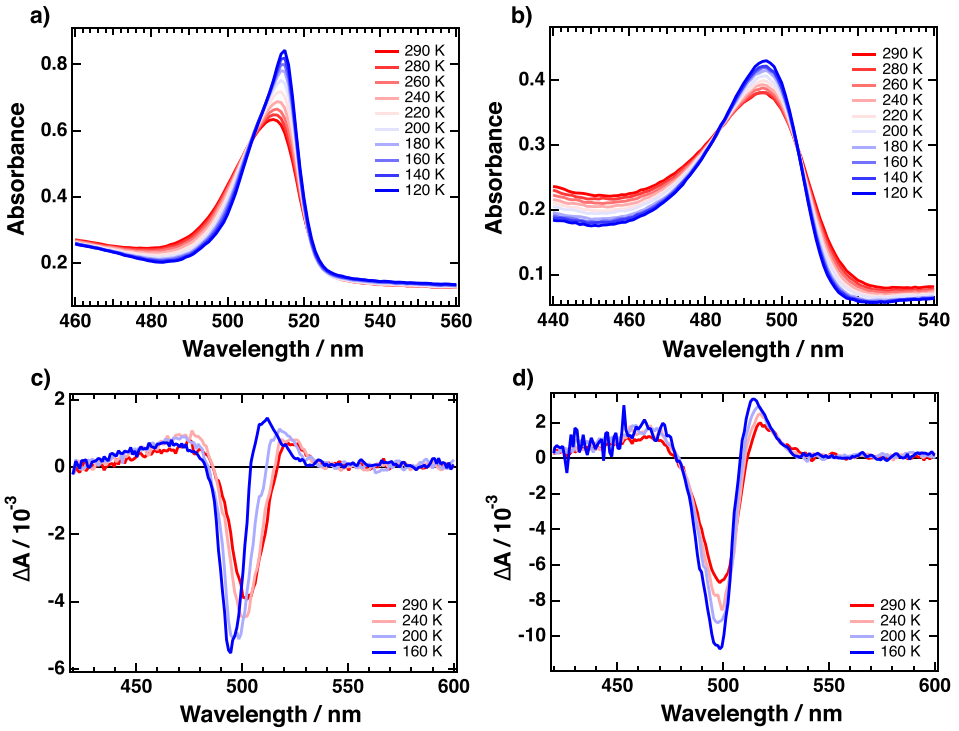

Figure 4. Temperature-dependent steady-state absorption spectra and temperature-dependent TA spectra of 2D perovskites incorporating PDMA (a,c) and PDEA (b,d). For the TA spectra, the samples were excited at 390 nm with a fluence of 10 uJ/cm^2, and the traces shown were taken at 0.5 ps after photoexcitation.

transfer excitons (CTEs) across the organic spacer layer. The features exhibited in the TA spectra of the PDEA sample corroborate this (Figure 1d). However, the relative contribution of the Stark effect is different depending on the spacer. When comparing the spectra of PDMA and PDEA-based materials, it is evident that the relative intensity of the Stark effect feature compared to the bleaching is lower for the PDEA than for the PDMA sample. This can be rationalized by the longer alkyl chain length in the PDEA spacer, which increases the interlayer distance and reduces the local electric field generated upon CTE formation.[30] This lower field can then lead to a reduction in the photoinduced Stark effect.

In both samples, the formation of CTEs occurs within the instrument response (<100 fs). By conducting a global analysis of the data, fitting with triexponential functions (Figure 2 and Figure S3, SI), the lifetime of the CTEs appears to be linked to the interlayer distance. Once formed, CTEs can either undergo separation into free charges or recombine. The CTEs were found to have a lifetime of 240 fs in the PDMA-based system, compared to 350 fs for the PDEA-based one; this difference could be attributed to the smaller spacer resulting in the charges being less spatially separated and thus making charge recombination faster. The two other components in the global fit correspond to the ground state bleaching and stimulated emission, contributing to the negative feature at 508 nm.

To corroborate this further, the electroabsorption (EA) spectra were measured (Figure 3a,b). They feature the same shape as the TA spectra, confirming the hypothesis that charge transfer excitons are photogenerated, resulting in a transient Stark effect. In addition, by comparison of the signal obtained in the voltage-dependent EA measurements (Figure 3c,d) to that in the TA spectra, it is possible to estimate the strength of the photoinduced electric field generated between the perovskite layers in the TA measurements.

The voltage applied across the perovskite layer must be calculated to account for the decrease in potential across the aluminum oxide. This layer is necessary to conduct the measurements, as it ensures that the perovskite is not oxidized or reduced at the FTO interface. The following equation[32] can be used to calculate the voltage drop across the perovskite layer (eq 4):

$$\Delta U_i = U_{app} \cdot \frac{d_i}{\varepsilon_i} \cdot \frac{1}{\sum \frac{d_i}{\varepsilon_i}} \tag{4}$$

where U_{app} is the applied potential, d_i the thickness of layer i (obtained via cross-sectional SEM images, Figure S4, SI), and ε_i the relative permittivity of the material (taken as 9 for Al_2O_3[33] and 25 for the perovskite[34,35]).

Since the positive peak at 520 nm in the PDMA TA spectrum only contains contributions from the transient Stark effect, the signal obtained in the TA measurement would correspond to an applied potential of 2.1 V and a photoinduced electric field of 10.2×10^4 Vcm^{-1}. Comparatively, the photoinduced electric field in PDEA is 0.35×10^4 Vcm^{-1}. This difference can be rationalized by the larger spacer in the PDEA sample resulting in an increased distance between the electron and hole which make up the charge transfer exciton.

Having established the impact of the spacer size on the formation of charge transfer excitons, we conducted temperature-dependent steady state absorption and TA measurements on the DJ phase. The steady-state absorption spectra of the PDMA-based system (Figure 4a) suggest a decrease in the broadening of the excitonic band upon lowering the temperature, which has been seen previously.[36]

In the TA spectra, the peaks at 500 nm decrease as the temperature decreases, whereas the peak at 520 nm increases in intensity while undergoing a blue shift that is more apparent

https://doi.org/10.1021/acs.jpclett.3c01125
J. Phys. Chem. Lett. 2023, 14, 6248−6254

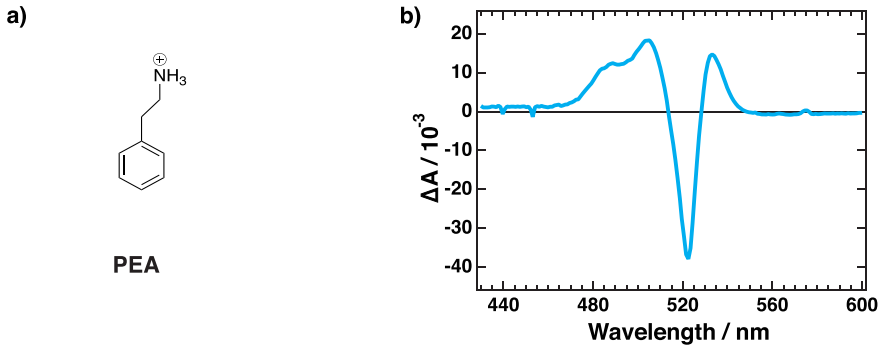

Figure 5. (a) Chemical structure of the 2-phenylethylammonium (PEA) spacer cation. (b) Transient absorption spectrum taken at 0.5 ps of PEA at a temperature of 160 K, exciting at 390 nm with a fluence of 10 uJ/cm^2.

in the PDMA than in the PDEA-based samples. The shift can be explained by the narrowing or sharpening of the excitonic peak in the absorption spectrum at lower temperatures. This also explains why the change is less pronounced for the PDEA, as its absorption spectrum narrows to a lesser extent than for the PDMA system. The increase in intensity is due to an increase in the transient Stark effect, which can be explained by crystal contraction upon the lowering of the temperature, resulting in a decrease in the interlayer spacing.[37] Therefore, the strength of the photoinduced electric field increased, yielding an increase in the positive signal in both cases. This further corroborates the difference in the transient Stark effect between the PDMA and PDEA samples (Figure 1c,d) due to the difference in spacer size. We can determine that as the temperature decreases from 290 to 160 K, the strength of the intrinsic electric field generated increases for PDMA-based samples, implying a decrease in the interlayer distance. Furthermore, the intrinsic electric field increases linearly as the temperature decreases; therefore, the charge transfer exciton size decreases linearly. There is a similar increase in the intrinsic electric field in the PDEA sample upon decreasing the temperature, in accordance with the assumptions. Due to the limitation of the time resolution of our TA setup, it is not possible to determine the impact of this decrease in the distance on the CTE formation. However, global analysis indicates that the lifetime of the CTEs increases with decreasing temperature (Figure S5, SI). This can be explained by a reduction in electron−phonon coupling as the temperature drops, resulting in a delay in CTE recombination.

These effects are assumed to be further pronounced for alternative 2D perovskite configurations such as in RP phases. We thus analyzed the 2-phenylethylammonium (PEA) spacer material (Figure 5a) that forms RP perovskites.[23] The steady-state absorption spectrum reveals n = 1 phase pure samples, similar to the DJ phases, while the TA spectrum exhibited the characteristic photoinduced Stark effect feature resulting from CTE formation (Figure S6). Compared to the PDMA DJ perovskite, the CTE lifetime was longer (500 fs vs 240 fs), in accordance with the increase in the interlayer distance.

While the phase identity appears to have little impact on the room-temperature TA and steady-state absorption spectra of RP and DJ congeners, the temperature-dependent TA measurements of the PEA-based 2D perovskite sample reveal a new feature at 485 nm at low temperature, which is not seen in the DJ samples (Figure 5b). By fitting the TA spectra at 0.5 ps obtained at room temperature and 160 K with a linear combination of the first and second derivative of the absorption spectra, we can estimate that there is a 30% increase in the contribution of the first derivative to the fit at 160 K when compared to the room temperature measurement. This indicates a contribution to the TA spectrum arising from the quantum confined Stark effect (QCSE) as the temperature decreases, which is not present in the DJ phase perovskites. This QCSE contribution can also explain the red shift in the negative peak upon lowering the temperature, further in accordance with the interlayer spacing and configuration.[25,38]

In summary, we have used transient absorption (TA) and electroabsorption (EA) spectroscopy to explore charge transfer excitons in 2D perovskites employing different spacer sizes in Ruddlesden−Popper (RP) and Dion−Jacobson (DJ) perovskite architectures. The TA spectra showed an apparent Stark effect in both DJ and RP-phase samples arising from the formation of charge transfer excitons within 100 fs after photoexcitation. By comparison of the spectra, it was possible to determine that the strength of the photoinduced Stark effect was dependent on the size of the spacer, with smaller spacers resulting in a more extensive transient Stark effect feature. However, the smaller spacers also exhibited a shorter charge transfer exciton (CTE) lifetime. By combining TA with EA spectroscopy, we could determine the photoinduced electric field generated within the samples, where it was shown that a field of 10.2×10^4 V cm^{-1} is produced upon CTE formation in PDMA-based 2D perovskites. This value decreases as the spacer size increases. Finally, temperature-dependent steady-state absorption and TA spectroscopy demonstrate an increase in the photoinduced Stark effect due to crystal contraction, accompanied by an increase in the CTE lifetime. Further comparison with RP-phase perovskites revealed a new peak in the TA spectra at low temperatures, attributed to a contribution from the quantum-confined Stark effect emerging from the structural change. This study provides insights into the impact of the structural characteristics of the spacer in layered (2D) hybrid perovskites on their photophysics, stimulating further investigations toward utilizing these effects in advanced material design and their application.

■ ASSOCIATED CONTENT

Data Availability Statement

The data presented here can be accessed at https://doi.org/10.5281/zenodo.7967407 (Zenodo) under the license CC-BY-4.0 (Creative Commons Attribution-ShareAlike 4.0 International).

Supporting Information

The Supporting Information is available free of charge at https://pubs.acs.org/doi/10.1021/acs.jpclett.3c01125.

https://doi.org/10.1021/acs.jpclett.3c01125
J. Phys. Chem. Lett. 2023, 14, 6248−6254

Materials and Methods, Results from Global Fitting of Transient Absorption Spectra, Supplementary UV/vis Absorption and Transient Absorption Spectra, Cross-Sectional SEM Images (PDF)

AUTHOR INFORMATION

Corresponding Authors

Jacques-E. Moser − *Photochemical Dynamics Group, Institute of Chemical Sciences and Engineering, École Polytechnique Fédérale de Lausanne, 1015 Lausanne, Switzerland;* orcid.org/0000-0003-0747-4666; Email: je.moser@epfl.ch

Jovana V. Milić − *Laboratory of Photonics and Interfaces, Institute of Chemical Sciences and Engineering, École Polytechnique Fédérale de Lausanne, 1015 Lausanne, Switzerland; Adolphe Merkle Institute, University of Fribourg, 1700 Fribourg, Switzerland;* orcid.org/0000-0002-9965-3460; Email: jovana.milic@unifr.ch

Authors

George C. Fish − *Photochemical Dynamics Group, Institute of Chemical Sciences and Engineering, École Polytechnique Fédérale de Lausanne, 1015 Lausanne, Switzerland*

Aaron T. Terpstra − *Photochemical Dynamics Group, Institute of Chemical Sciences and Engineering, École Polytechnique Fédérale de Lausanne, 1015 Lausanne, Switzerland*

Algirdas Dučinskas − *Laboratory of Photonics and Interfaces, Institute of Chemical Sciences and Engineering, École Polytechnique Fédérale de Lausanne, 1015 Lausanne, Switzerland; Max Planck Institute for Solid State Research, 70569 Stuttgart, Germany*

Masaud Almalki − *Laboratory of Photonics and Interfaces, Institute of Chemical Sciences and Engineering, École Polytechnique Fédérale de Lausanne, 1015 Lausanne, Switzerland*

Loï C. Carbone − *Laboratory of Photonics and Interfaces, Institute of Chemical Sciences and Engineering, École Polytechnique Fédérale de Lausanne, 1015 Lausanne, Switzerland*

Lukas Pfeifer − *Laboratory of Photonics and Interfaces, Institute of Chemical Sciences and Engineering, École Polytechnique Fédérale de Lausanne, 1015 Lausanne, Switzerland;* orcid.org/0000-0002-8461-3909

Michael Grätzel − *Laboratory of Photonics and Interfaces, Institute of Chemical Sciences and Engineering, École Polytechnique Fédérale de Lausanne, 1015 Lausanne, Switzerland;* orcid.org/0000-0002-0068-0195

Complete contact information is available at: https://pubs.acs.org/10.1021/acs.jpclett.3c01125

Author Contributions

The manuscript was written by G.F. with the support of other coauthors. G.F. and J.E.M. led the study and analyzed it with the support of other coauthors. G.F. performed transient absorption and electro-absorption spectroscopy and the analysis, A.D. and M.A. prepared thin films and characterized them structurally under the supervision of J.V.M. and M.G., while L.C.C. synthesized and characterized the organic spacers under the supervision of L.P. and J.V.M. J.E.M. and J.V.M. directed the project. All authors approved the final manuscript.

Notes

The authors declare no competing financial interest.

ACKNOWLEDGMENTS

G.C.F. and J.E.M. acknowledge financial support from the Swiss National Science Foundation (Grant no. 200021_175729) and the National Center of Competence in Research "Molecular Ultrafast Science and Technology" (NCCR-MUST). J.V.M. acknowledges the support of the Swiss National Science Foundation (Grant no. 193174). A.D. is grateful to the Max Planck-EPFL Center for support.

REFERENCES

(1) Saparov, B.; Mitzi, D. B. Organic-Inorganic Perovskites: Structural Versatility for Functional Materials Design. *Chem. Rev.* **2016**, *116*, 4558−4596.

(2) Grancini, G.; Nazeeruddin, M. K. Dimensional Tailoring of Hybrid Perovskites for Photovoltaics. *Nat. Rev. Mater.* **2019**, *4*, 4−22.

(3) Jena, A. K.; Kulkarni, A.; Miyasaka, T. Halide Perovskite Photovoltaics: Background, Status, and Future Prospects. *Chem. Rev.* **2019**, *119*, 3036−3103.

(4) Jeong, J.; Kim, M.; Seo, J.; Lu, H.; Ahlawat, P.; Mishra, A.; Yang, Y.; Hope, M. A.; Eickemeyer, F. T.; Kim, M.; Yoon, Y. J.; Choi, I. W.; Darwich, B. P.; Choi, S. J.; Jo, Y.; Lee, J. H.; Walker, B.; Zakeeruddin, S. M.; Emsley, L.; Rothlisberger, U.; Hagfeldt, A.; Kim, D. S.; Grätzel, M.; Kim, J. Y. Pseudo-Halide Anion Engineering for α-$FAPbI_3$ Perovskite Solar Cells. *Nature* **2021**, *592*, 381−385.

(5) Kim, Y. H.; Kim, S.; Kakekhani, A.; Park, J.; Park, J.; Lee, Y. H.; Xu, H.; Nagane, S.; Wexler, R. B.; Kim, D. H.; Jo, S. H.; Martínez-Sarti, L.; Tan, P.; Sadhanala, A.; Park, G. S.; Kim, Y. W.; Hu, B.; Bolink, H. J.; Yoo, S.; Friend, R. H.; Rappe, A. M.; Lee, T. W. Comprehensive Defect Suppression in Perovskite Nanocrystals for High-Efficiency Light-Emitting Diodes. *Nat. Photonics* **2021**, *15*, 148−155.

(6) Das, S.; Gholipour, S.; Saliba, M. Perovskites for Laser and Detector Applications. *Energy Environ. Mater.* **2019**, *2*, 146−153.

(7) Pellet, N.; Gao, P.; Gregori, G.; Yang, T. Y.; Nazeeruddin, M. K.; Maier, J.; Grätzel, M. Mixed-Organic-Cation Perovskite Photovoltaics for Enhanced Solar-Light Harvesting. *Angew. Chem., Int. Ed. Engl.* **2014**, *53*, 3151−3157.

(8) Saliba, M.; Matsui, T.; Seo, J. Y.; Domanski, K.; Correa-Baena, J. P.; Nazeeruddin, M. K.; Zakeeruddin, S. M.; Tress, W.; Abate, A.; Hagfeldt, A.; Grätzel, M. Cesium-Containing Triple Cation Perovskite Solar Cells: Improved Stability, Reproducibility and High Efficiency. *Energy Environ. Sci.* **2016**, *9*, 1989−1997.

(9) Noh, J. H.; Im, S. H.; Heo, J. H.; Mandal, T. N.; Seok, S. il. Chemical Management for Colorful, Efficient, and Stable Inorganic-Organic Hybrid Nanostructured Solar Cells. *Nano Lett.* **2013**, *13*, 1764−1769.

(10) Wang, R.; Mujahid, M.; Duan, Y.; Wang, Z.-K.; Xue, J.; Yang, Y. A Review of Perovskites Solar Cell Stability. *Adv. Func. Mat.* **2019**, *29*, 1808843.

(11) Ducinskas, A.; Kim, G. Y.; Moia, D.; Senocrate, A.; Wang, Y.-R.; Hope, M. A.; Mishra, A.; Kubicki, D. J.; Siczek, M.łło.; Bury, W.; Schneeberger, T.; Emsley, L.; Milic, J. V.; Maier, J.; Gratzel, M. Unravelling the Behavior of Dion−Jacobson Layered Hybrid Perovskites in Humid Environments. *ACS Energy Lett.* **2021**, *6* (2), 337−344.

(12) Ye, J.; Zheng, H.; Zhu, L.; Liu, G.; Zhang, X.; Hayat, T.; Pan, X.; Dai, S. Enhanced Moisture Stability of Perovskite Solar Cells with Mixed-Dimensional and Mixed-Compositional Light-Absorbing Materials. *Sol. RRL* **2017**, *1*, 1700125.

(13) Garai, R.; Gupta, R. K.; Hossain, M.; Iyer, P. K. Surface Recrystallized Stable 2D−3D Graded Perovskite Solar Cells for Efficiency beyond 21. *J. Mater. Chem. A* **2021**, *9*, 26069−26076.

(14) Li, X.; Hoffman, J. M.; Kanatzidis, M. G. The 2D Halide Perovskite Rulebook: How the Spacer Influences Everything from the

Structure to Optoelectronic Device Efficiency. *Chem. Rev.* **2021**, *121*, 2230−2291.
(15) Soe, C. M. M.; Stoumpos, C. C.; Kepenekian, M.; Traoré, B.; Tsai, H.; Nie, W.; Wang, B.; Katan, C.; Seshadri, R.; Mohite, A. D.; Even, J.; Marks, T. J.; Kanatzidis, M. G. New Type of 2D Perovskites with Alternating Cations in the Interlayer Space, $(C(NH_2)_3)(CH_3NH_3)NPb_nI_{3n+1}$: Structure, Properties, and Photovoltaic Performance. *J. Am. Chem. Soc.* **2017**, *139*, 16297−16309.
(16) Yang, J.; Yang, T.; Liu, D.; Zhang, Y.; Luo, T.; Lu, J.; Fang, J.; Wen, J.; Deng, Z.; Liu, S.; Chen, L.; Zhao, K. Stable 2D Alternating Cation Perovskite Solar Cells with Power Conversion Efficiency > 19% via Solvent Engineering. *Sol. RRL* **2021**, *5*, 2100286.
(17) Gao, X.; Zhang, X.; Yin, W.; Wang, H.; Hu, Y.; Zhang, Q.; Shi, Z.; Colvin, V. L.; Yu, W. W.; Zhang, Y. Ruddlesden−Popper Perovskites: Synthesis and Optical Properties for Optoelectronic Applications. *Adv. Sci.* **2019**, *6*, 1900941.
(18) Mao, L.; Ke, W.; Pedesseau, L.; Wu, Y.; Katan, C.; Even, J.; Wasielewski, M. R.; Stoumpos, C. C.; Kanatzidis, M. G. Hybrid Dion-Jacobson 2D Lead Iodide Perovskites. *J. Am. Chem. Soc.* **2018**, *140* (10), 3775−3783.
(19) Blancon, J. C.; Even, J.; Stoumpos, C. C.; Kanatzidis, M. G.; Mohite, A. D. Semiconductor Physics of Organic−Inorganic 2D Halide Perovskites. *Nat. Nanotechnol.* **2020**, *15*, 969−985.
(20) Hu, Y.; Spies, L. M.; Alonso-Álvarez, D.; Mocherla, P.; Jones, H.; Hanisch, J.; Bein, T.; Barnes, P. R. F.; Docampo, P. Identifying and Controlling Phase Purity in 2D Hybrid Perovskite Thin Films. *J. Mater. Chem. A* **2018**, *6*, 22215−22225.
(21) Cao, D. H.; Stoumpos, C. C.; Farha, O. K.; Hupp, J. T.; Kanatzidis, M. G. 2D Homologous Perovskites as Light-Absorbing Materials for Solar Cell Applications. *J. Am. Chem. Soc.* **2015**, *137*, 7843−7850.
(22) Yuan, Z.; Shu, Y.; Xin, Y.; Ma, B. Highly Luminescent Nanoscale Quasi-2D Layered Lead Bromide Perovskites with Tunable Emissions. *Chem. Commun.* **2016**, *52*, 3887−3890.
(23) Qin, C.; Xu, L.; Zhou, Z.; Song, J.; Ma, S.; Jiao, Z.; Jiang, Y. Carrier Dynamics in Two-Dimensional Perovskites: Dion−Jacobson vs. Ruddlesden−Popper Thin Films. *J. Mater. Chem. A* **2022**, *10*, 3069−3076.
(24) Milić, J. V. Multifunctional Layered Hybrid Perovskites. *J. Mater. Chem. C* **2021**, *9*, 11428−11443.
(25) Walters, G.; Wei, M.; Voznyy, O.; Quintero-Bermudez, R.; Kiani, A.; Smilgies, D. M.; Munir, R.; Amassian, A.; Hoogland, S.; Sargent, E. The Quantum-Confined Stark Effect in Layered Hybrid Perovskites Mediated by Orientational Polarizability of Confined Dipoles. *Nat. Commun.* **2018**, *9*, 4214.
(26) Burgos-Caminal, A.; Socie, E.; Bouduban, M. E. F.; Moser, J.-E. Exciton and Carrier Dynamics in Two-Dimensional Perovskites. *J. Phys. Chem. Lett.* **2020**, *11*, 7692−7701.
(27) Yin, J.; Naphade, R.; Maity, P.; Gutiérrez-Arzaluz, L.; Almalawi, D.; Roqan, I. S.; Brédas, J. L.; Bakr, O. M.; Mohammed, O. F. Manipulation of Hot Carrier Cooling Dynamics in Two-Dimensional Dion−Jacobson Hybrid Perovskites via Rashba Band Splitting. *Nat. Commun.* **2021**, *12*, 3995.
(28) Li, Y.; Milić, J. V.; Ummadisingu, A.; Seo, J. Y.; Im, J. H.; Kim, H. S.; Liu, Y.; Dar, M. I.; Zakeeruddin, S. M.; Wang, P.; Hagfeldt, A.; Grätzel, M. Bifunctional Organic Spacers for Formamidinium-Based Hybrid Dion-Jacobson Two-Dimensional Perovskite Solar Cells. *Nano Lett.* **2019**, *19*, 150−157.
(29) Gélvez-Rueda, M. C.; Ahlawat, P.; Merten, L.; Jahanbakhshi, F.; Mladenović, M.; Hinderhofer, A.; Dar, M. I.; Li, Y.; Dučinskas, A.; Carlsen, B.; Tress, W.; Ummadisingu, A.; Zakeeruddin, S. M.; Schreiber, F.; Hagfeldt, A.; Rothlisberger, U.; Grozema, F. C.; Milić, J. V.; Grätzel, M. Formamidinium-Based Dion-Jacobson Layered Hybrid Perovskites: Structural Complexity and Optoelectronic Properties. *Adv. Funct. Mater.* **2020**, *30*, 2003428.
(30) Dučinskas, A.; Fish, G. C.; Hope, M. A.; Merten, L.; Moia, D.; Hinderhofer, A.; Carbone, L. C.; Moser, J.-E.; Schreiber, F.; Maier, J.; Milić, J. V.; Grätzel, M. The Role of Alkyl Chain Length and Halide Counter Ion in Layered Dion-Jacobson Perovskites with Aromatic Spacers. *J. Phys. Chem. Lett.* **2021**, *12*, 10325−10332.
(31) Bouduban, M. E. F.; Burgos-Caminal, A.; Teuscher, J.; Moser, J.-E. Unveiling the Nature of Charge Carrier Interactions by Electroabsorption Spectroscopy: An Illustration with Lead-Halide Perovskites. *Chimia* **2017**, *71*, 231−235.
(32) Paraecattil, A. A.; de Jonghe-Risse, J.; Pranculis, V.; Teuscher, J.; Moser, J. E. Dynamics of Photocarrier Separation in $MAPbI_3$ Perovskite Multigrain Films under a Quasistatic Electric Field. *J. Phys. Chem. C* **2016**, *120*, 19595−19602.
(33) Tanner, C. M.; Perng, Y. C.; Frewin, C.; Saddow, S. E.; Chang, J. P. Electrical Performance of Al_2O_3 Gate Dielectric Films Deposited by Atomic Layer Deposition on 4H-SiC. *Appl. Phys. Lett.* **2007**, *91*, 203510.
(34) Zhang, X.; Ren, X.; Liu, B.; Munir, R.; Zhu, X.; Yang, D.; Li, J.; Liu, Y.; Smilgies, D. M.; Li, R.; Yang, Z.; Niu, T.; Wang, X.; Amassian, A.; Zhao, K.; Liu, S. Stable High Efficiency Two-Dimensional Perovskite Solar Cells via Cesium Doping. *Energy Environ. Sci.* **2017**, *10*, 2095−2102.
(35) Shao, M.; Bie, T.; Yang, L.; Gao, Y.; Jin, X.; He, F.; Zheng, N.; Yu, Y.; Zhang, X. Over 21% Efficiency Stable 2D Perovskite Solar Cells. *Adv. Mater.* **2022**, *34*, 2107211.
(36) Zhang, Y.; Wang, R.; Li, Y.; Wang, Z.; Hu, S.; Yan, X.; Zhai, Y.; Zhang, C.; Sheng, C. X. Optical Properties of Two-Dimensional Perovskite Films of $(C_6H_5C_2H_4NH_3)_2[PbI_4]$ and $(C_6H_5C_2H_4NH_3)_2(CH_3NH_3)_2[Pb_3I_{10}]$. *J. Phys. Chem. Lett.* **2019**, *10*, 13−19.
(37) Wang, S.; Ma, J.; Li, W.; Wang, J.; Wang, H.; Shen, H.; Li, J.; Wang, J.; Luo, H.; Li, D. Temperature-Dependent Band Gap in Two-Dimensional Perovskites: Thermal Expansion Interaction and Electron−Phonon Interaction. *J. Phys. Chem. Lett.* **2019**, *10*, 2546−2553.
(38) Queloz, V. I. E.; Bouduban, M. E. F.; García-Benito, I.; Fedorovskiy, A.; Orlandi, S.; Cavazzini, M.; Pozzi, G.; Trivedi, H.; Lupascu, D. C.; Beljonne, D.; Moser, J.-E.; Nazeeruddin, M. K.; Quarti, C.; Grancini, G. Spatial Charge Separation as the Origin of Anomalous Stark Effect in Fluorous 2D Hybrid Perovskites. *Adv. Funct. Mater.* **2020**, *30*, 2000228.

https://doi.org/10.1021/acs.jpclett.3c01125
J. Phys. Chem. Lett. 2023, 14, 6248−6254

Supplementary Information

The Impact of Spacer Size on Charge Transfer Excitons in Dion-Jacobson and Ruddlesden-Popper Layered Hybrid Perovskites

George C. Fish,[†] Aaron T. Terpstra,[†] Algirdas Dučinskas,[‡#] Masaud Almalki,[‡] Loï C. Carbone,[‡] Lukas Pfeifer,[‡] Michael Grätzel,[‡] Jacques-E. Moser,[†] and Jovana V. Milić [‡§]**

[†] Photochemical Dynamics Group, Institute of Chemical Sciences and Engineering, École Polytechnique Fédérale de Lausanne, 1015 Lausanne, Switzerland.

[‡] Laboratory of Photonics and Interfaces, Institute of Chemical Sciences and Engineering, École Polytechnique Fédérale de Lausanne, 1015 Lausanne, Switzerland

[#] Max Planck Institute for Solid State Research, 70569 Stuttgart, Germany

[§] Adolphe Merkle Institute, University of Fribourg, 1700 Fribourg, Switzerland

The data presented here can be accessed at DOI:10.5281/zenodo.7967407 (Zenodo)

Experimental Methods

Sample Preparation

The 2D perovskite samples have been previously synthesized and characterized.[1–3] PDMA and PDEA Dion-Jacobson samples were prepared by dissolving either $PDMAI_2$ or $PDEAI_2$ in a 1:1 ratio with PbI_2 in a mixture of DMSO and DMF (4:1 volumetric ratio). The PEA Ruddlesden-Popper samples were prepared by dissolving either PEAI in a 2:1 ratio with PbI_2 in the same solvent mixture. Solutions were heated to 60 °C and spin-cast onto glass substrates before annealing at 150 °C for 10 min.

Samples for EA were fabricated by first depositing Al_2O_3, via atomic layer deposition, on FTO patterned glass substrates, before spin coating the same perovskite solutions as above. Finally, a gold electrode was deposited by thermal evaporation.

Spectroscopy

Absorption spectra were measured using a PerkinElmer Lambda 950 UV/vis/NIR spectrophotometer.

Transient absorption (TA) and electroabsorption (EA) spectra were measured using a femtosecond pump-probe spectrometer setup based on a Ti:sapphire laser (Clark-MXR, CPA-2001) delivering 778 nm pulses with a pulse width of 150 fs and a repetition rate of 1 kHz. For the TA measurements, the second harmonic of the fundamental (389 nm) was generated by passing the fundamental through a beta-barium borate (BBO) crystal yielding the pump beam. The probe, a broadband white light continuum, was generated by passing part of the fundamental through a 5 mm-thick oscillating CaF_2 plate (for TA, 450 – 1050 nm) or through a 4 mm-thick sapphire window (for EA, 400 – 750 nm). For TA, the pump and probe were set at magic angle polarisation, and samples were measured in transmission mode. Meanwhile, for EA, samples were measured in reflection mode. In both cases, the probe was split into a signal beam passing through the sample and a reference beam to account for shot-to-shot fluctuations. The signal and reference beams were dispersed in two respective grating spectrographs (SpectraPro 2500i, Princeton Instruments or SR163, Andor Instruments) and detected shot-to-shot at 1 kHz by 512x58 pixel back-thinned charge-coupled device cameras (Hamamatsu S07030-0906). For TA measurements, a chopper was set at 500 Hz to modulate the pump beam's frequency, enabling absorption with and without the pump to be acquired in the exact measurement. Similarly, for EA measurements, the electric field across the sample was modulated at half the amplifier frequency (500 Hz), using square pulses generated by a function generator (Tektronix AFG 2021, -10 to 10 V, 100 μs pulse duration). The current responses across the samples were recorded using a 50 Ω series load with a 400 MHz bandpass oscilloscope (Tektronix TDS 3044B).

Temperature-dependent measurements were carried out using a cryostat (Oxford Instruments).

Supplementary Data

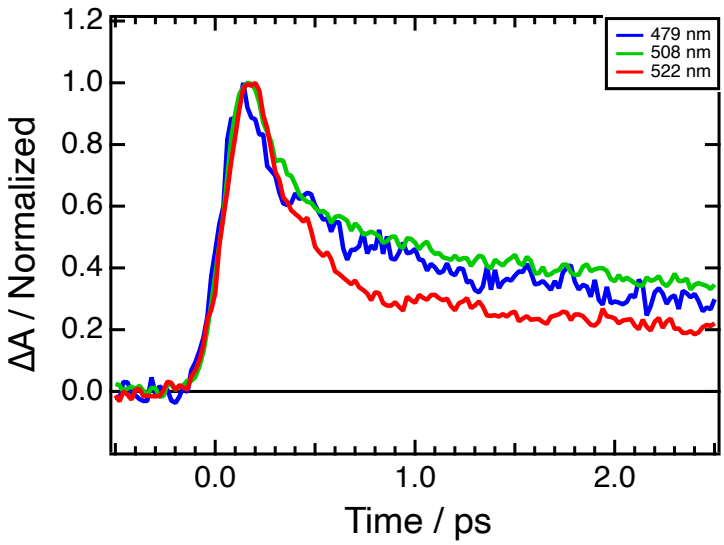

Figure S1. Kinetic traces for the three features in the transient absorption spectrum (at 479, 508, and 522 nm) of PDMA-based samples normalized to show the similarity of the early time dynamics for the three features.

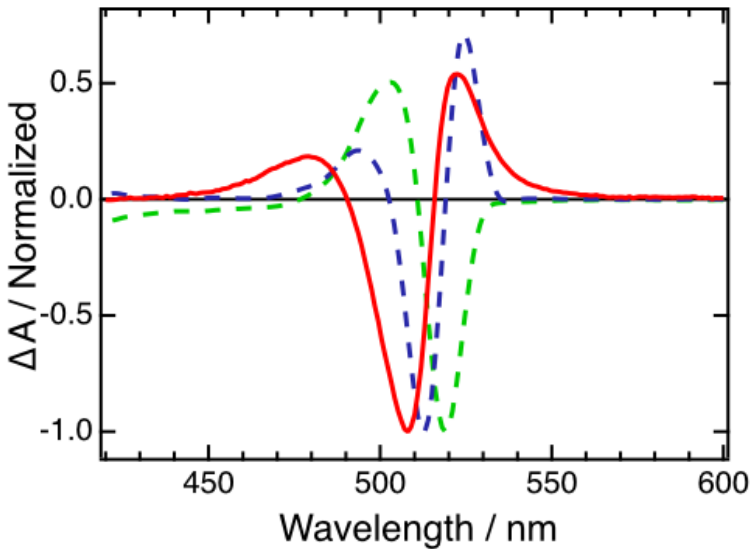

Figure S2. Normalized transient absorption of PDMA-based samples (red) alongside the first (green) and second (blue) derivatives of the absorption spectrum.

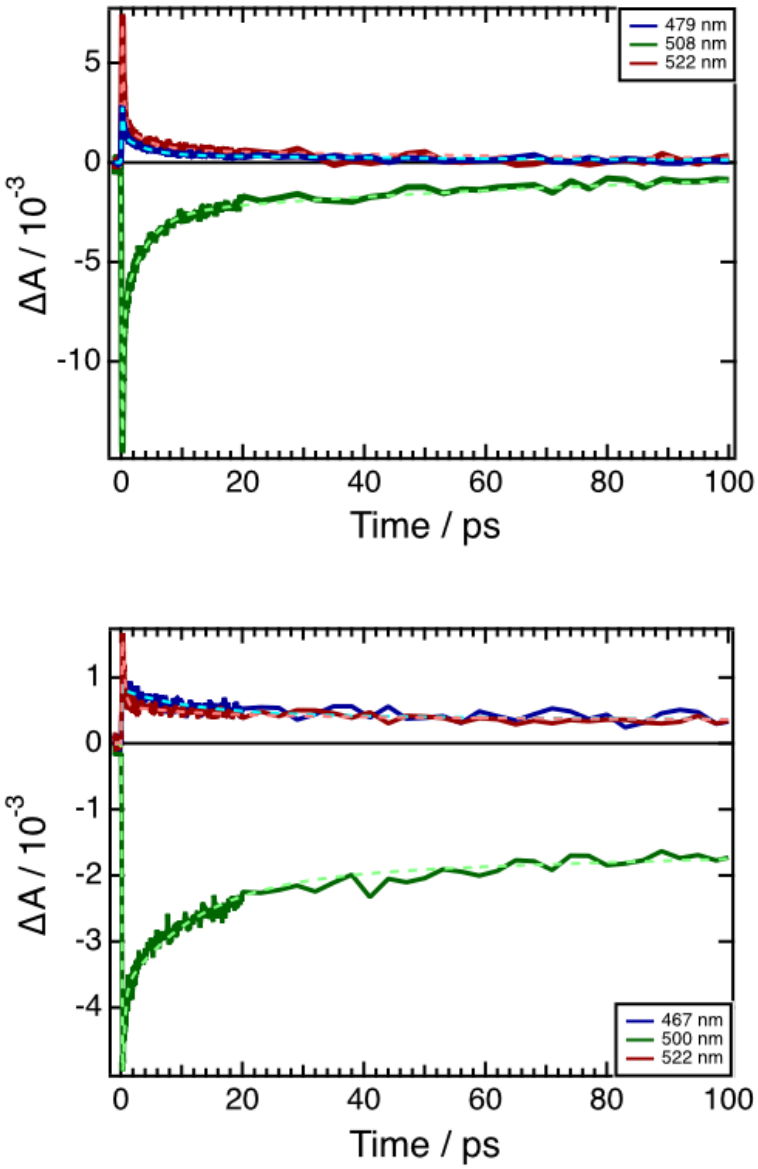

Figure S3. Kinetic traces for the three peaks in the transient absorption spectra of PDMA (top) and PDEA (bottom) based samples fitted with the result from the global fitting procedure (dashed line).

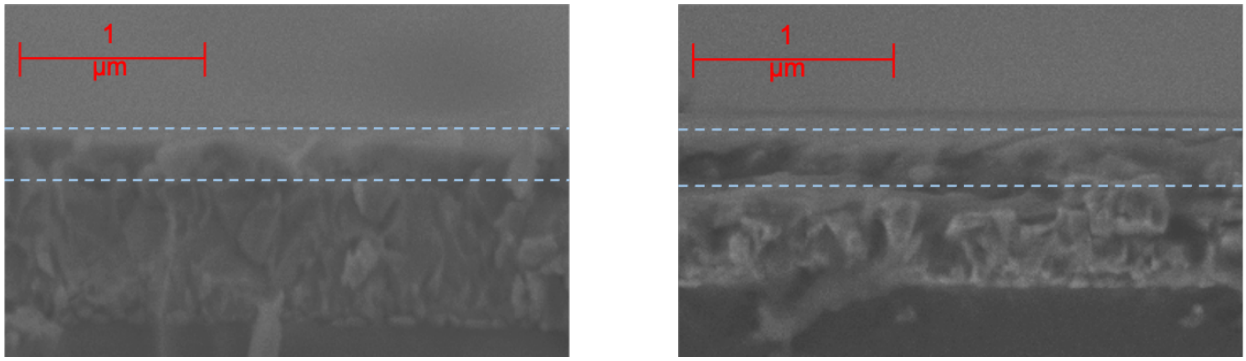

Figure S4. Cross-sectional scanning electron microscopy (SEM) images of 2D perovskite incorporating PDMA (left) and PDEA (right) spacers. The samples were the same as used for the electroabsorption measurements and had the following configuration: Glass/FTO/Al_2O_3/perovskite/Ag.

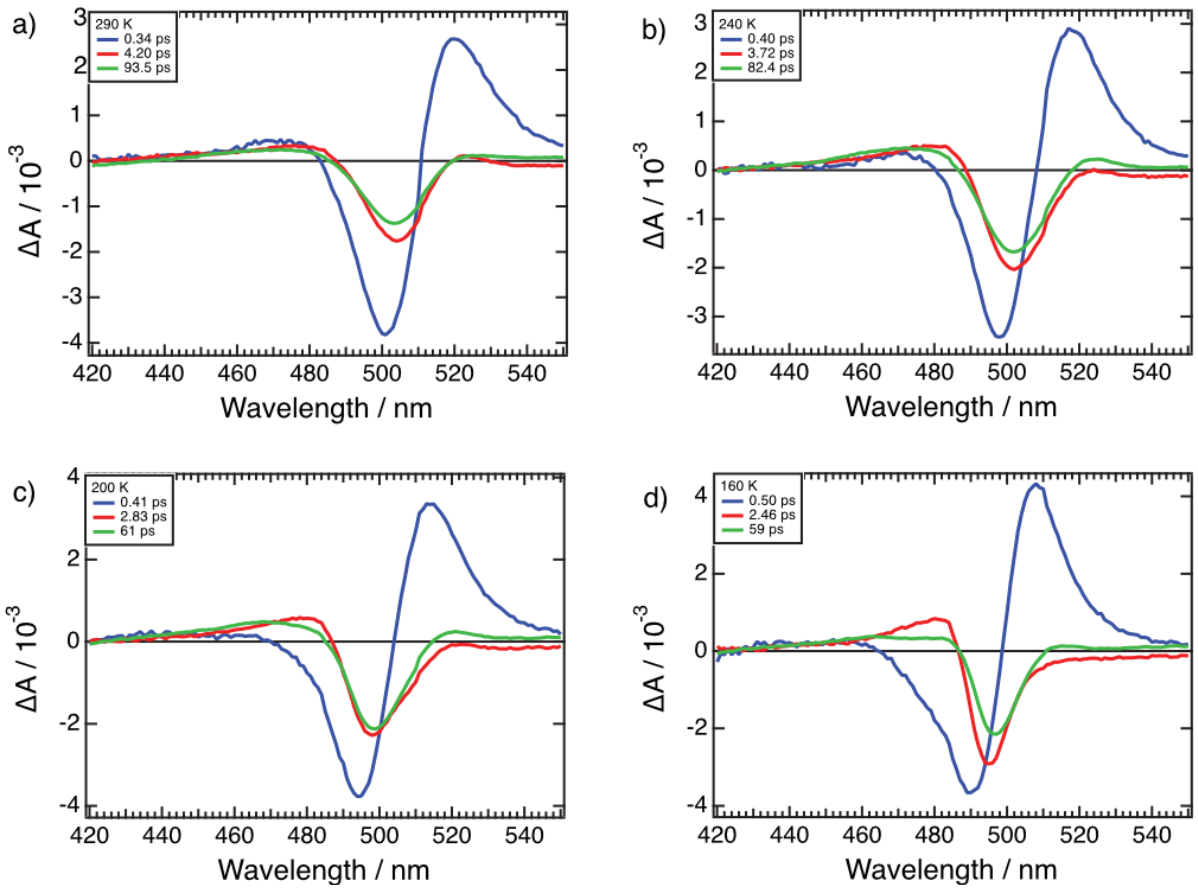

Figure S5. Decay-associated spectra (DAS) following global analysis on the TA spectra of PDMA-based samples at different temperatures.

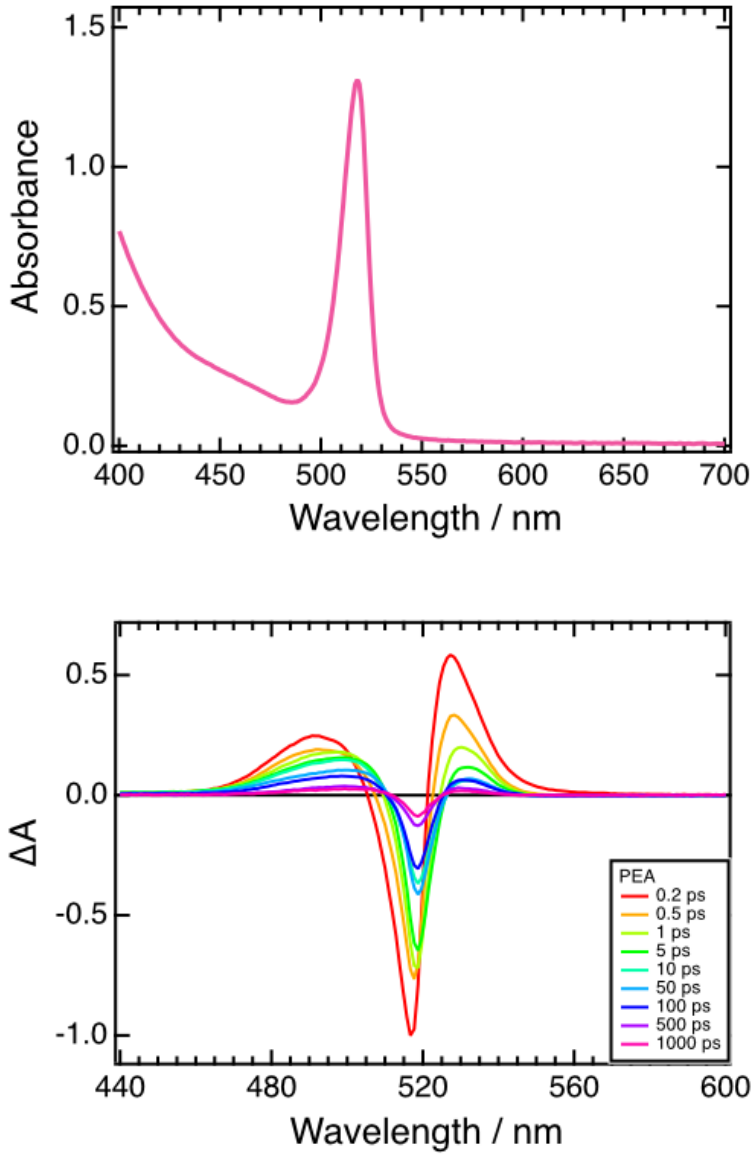

Figure S6. Steady-state absorption (top) and transient absorption (bottom) spectra of a 2D perovskite incorporating PEA as the spacer. For the TA, the sample was excited at 390 nm with a fluence of 10 uJ/cm^2.

References

(1) Li, Y.; Milić, J. v.; Ummadisingu, A.; Seo, J. Y.; Im, J. H.; Kim, H. S.; Liu, Y.; Dar, M. I.; Zakeeruddin, S. M.; Wang, P.; Hagfeldt, A.; Grätzel, M. Bifunctional Organic Spacers for Formamidinium-Based Hybrid Dion-Jacobson Two-Dimensional Perovskite Solar Cells. *Nano Lett* **2019**, *19*, 150–157. https://doi.org/10.1021/acs.nanolett.8b03552.

(2) Gélvez-Rueda, M. C.; Ahlawat, P.; Merten, L.; Jahanbakhshi, F.; Mladenović, M.; Hinderhofer, A.; Dar, M. I.; Li, Y.; Dučinskas, A.; Carlsen, B.; Tress, W.; Ummadisingu, A.; Zakeeruddin, S. M.; Schreiber, F.; Hagfeldt, A.; Rothlisberger, U.; Grozema, F. C.; Milić, J. v.; Graetzel, M. Formamidinium-Based Dion-Jacobson Layered Hybrid Perovskites: Structural Complexity and Optoelectronic Properties. *Adv. Func. Mater.* **2020**, *30*, 2003428. https://doi.org/10.1002/adfm.202003428.

(3) Dučinskas, A.; Fish, G. C.; Hope, M. A.; Merten, L.; Moia, D.; Hinderhofer, A.; Carbone, L. C.; Moser, J. E.; Schreiber, F.; Maier, J.; Milić, J. v.; Grätzel, M. The Role of Alkyl Chain Length and Halide Counter Ion in Layered Dion-Jacobson Perovskites with Aromatic Spacers. *J. Phys. Chem. Lett.* **2021**, *12*, 10325–10332. https://doi.org/10.1021/acs.jpclett.1c02937.